Angular distributions for near-threshold $(e,2e)$ processes for H, He, and other rare-gas targets

Cheng Pan and Anthony F. Starace
Department of Physics and Astronomy, The University of Nebraska, Lincoln, Nebraska 68588-0111
(Received 11 October 1991)

Distorted-wave calculations of the triply differential cross sections for electron-impact ionization of H, He, Ne, Ar, Kr, and Xe are presented for final-state electrons sharing ≤ 4 eV excess energy and for the coplanar, $\theta_{12}=\pi$ geometry. Results for H and He targets, presented briefly elsewhere [C. Pan and A. F. Starace, Phys. Rev. Lett. **67**, 185 (1991)], are analyzed in greater detail and compared with available experimental and other theoretical results. In particular, for He targets the effects of exchange and of second-order capture processes are exhibited. These are shown to be of lesser importance than other short-range effects on the s-wave phase shifts of both incident and final-state continuum electrons for reproducing the experimentally observed target dependence of the electron angular distributions for H and He targets [P. Schlemmer, T. Rösel, K. Jung, and H. Ehrhardt, Phys. Rev. Lett. **63**, 252 (1989)]. More approximate theoretical $(e,2e)$ results for Ne, Ar, Kr, and Xe targets also show striking target dependences; they are compared with available experimental results.

PACS number(s): 34.80.Dp

I. INTRODUCTION

The experimental and theoretical analysis of the triply differential cross sections for $(e,2e)$ processes is a sensitive means for elucidating the fundamental dynamics of three-body systems interacting via Coulomb forces [1–4]. Recent low-energy $(e,2e)$ experiments [5–8] for various targets have shown the triply differential cross sections to be highly dependent on the target even though at asymptotic separations the long-range fields in the final state are target independent. While the Wannier theory [9–12] for the threshold energy dependence has been analyzed for all contributing partial waves [13–15] only very recently have theoretical estimates of their relative importance, which are essential for describing the triply differential cross sections, been made [16–18]. In particular, Pan and Starace [17] showed (for the case in which the two electrons leave in opposite directions) that the experimentally observed [6] target dependence of near-threshold triply differential cross sections for $(e,2e)$ processes in H and He stems essentially from short-range effects on the s-wave phase shifts of both incident and final-state continuum electrons.

The theoretical treatment of $(e,2e)$ processes is difficult because there does not exist an analytic solution for the wave function for two electrons moving in a Coulomb field. While the asymptotic boundary condition that such a wave function should satisfy is known, incorporation of this boundary condition in numerical calculations has only recently been accomplished [19]. Further approximations to the exact wave functions are needed to make numerical calculations possible. Typically, especially in order to facilitate analytic treatments, the incident electron is described by a plane wave and the final-state continuum electrons are assumed to move in a point Coulomb potential. Neither of these approximations is accurate for low energies (i.e., near threshold) since the relative importance of low angular momentum partial-wave components in both initial and final wave functions increases at low energies. For H and He, it is predominantly the s-wave components which sample the structure of the target and thereby have phase shifts which carry information about the target [17]. Since our concern here is with the target dependence of near-threshold $(e,2e)$ processes, we focus mostly on the accurate treatment of such short-range interactions of the incident and final continuum electrons with the target. For the special case in which the two continuum electrons leave in opposite directions (i.e., $\theta_{12}=\pi$), we find empirically that a simple screening approximation for their mutual interaction suffices.

Another approximation typically made is to calculate continuum radial wave functions using local potentials to describe the interaction with the neutral or ionized target. In our calculations we wish to treat the target-dependent, short-range interactions as accurately as possible. We have therefore calculated radial wave functions in appropriately defined Hartree-Fock (i.e., direct and exchange) potentials. While this makes it difficult for us therefore to define a capture amplitude, capture processes are nevertheless to some extent included in our results.

Specifically, then, in this paper we give a more detailed presentation of our previously reported distorted-wave calculations [17] of the triply differential cross sections for $(e,2e)$ processes for H and He targets. We also present theoretical triply differential $(e,2e)$ results for other rare-gas targets. Whereas our prior numerical results for H and for He were only for the case of 4 eV excess energy [17], we report here results for 2 and 0.5 eV excess energy since there are also for these cases experimental data [5,16,20] with which we can compare. For H and for He, we compare our results in addition with the

recent theoretical calculations of Brauner *et al.* [16] and of Jones, Madison, and Srivastava [18]. For He, we present in addition detailed information on the role of exchange and capture processes and compare our findings with those of Jones, Madison, and Srivastava [18].

For the rare-gas atoms Ne, Ar, Kr, and Xe we present here results of more approximate distorted-wave calculations for near-threshold $(e,2e)$ triply differential cross sections. Our results for 4, 2, and 0.5 eV excess energy have angular distributions which are very different from those for H and He targets. They are compared with available experimental results [7,8].

In Sec. II we present a detailed description of our distorted-wave calculations. In Sec. III we present results of our calculations for 4, 2, and 0.5 eV excess energy for H and He targets and compare with available experimental and other theoretical results. In particular, differences in the absolute magnitudes of the various theoretical calculations are examined. In Sec. IV we present results of our calculations for 4, 2, and 0.5 eV excess energy for Ne, Ar, Kr, and Xe targets and compare with experimental results. In Sec. V we summarize our findings and present our conclusions. Finally, we note that for the equal-energy-sharing case with 2 eV excess energy we give in tabular form all of the theoretical parameters needed to reconstruct our $(e,2e)$ results for H, He, Ne, Ar, Kr, and Xe in order to facilitate comparisons with future experimental and theoretical results (cf. Table III).

II. THEORY

The general theory of $(e,2e)$ processes has recently been reviewed both by Byron and Joachain [3] and, for H atom targets, by Brauner, Briggs, and Klar [19]. Furthermore, parametrized forms for the angular distributions have been presented by Huang [21] and by Altick [22]. We focus here therefore on our *ab initio* theoretical approach for taking short-range interactions into account when calculating $(e,2e)$ triply differential cross sections.

A. General description of approximations used

For infinite nuclear mass, the differential cross section for electron-impact ionization [19] becomes (in a.u.)

$$\frac{d\sigma}{d\mathbf{k}_1 d\mathbf{k}_2}=\frac{(2\pi)^4}{k}|\langle\Psi_f^-|V|\Phi_i^+\rangle|^2\delta(E_f-E_i)\ . \tag{1}$$

In Eq. (1), k is the magnitude of the momentum of the incident electron, $\mathbf{k}_1$ and $\mathbf{k}_2$ are the momenta of the two continuum electrons in the final state, and E_i and E_f are the energies of the initial and final states. The perturbation V is the difference between the exact Hamiltonian and the approximate Hamiltonian used to construct Φ_i^+, the distorted wave used to describe approximately the initial state [23]. In our calculations V is defined approximately by

$$V=\sum_{i=1}^{N}\frac{1}{|\mathbf{r}_{N+1}-\mathbf{r}_i|}-V_{\rm HF}^{N+1}(\mathbf{r}_{N+1})\ , \tag{2}$$

where the first term on the right-hand side of Eq. (2) is the Coulomb interaction between the incident electron and the N target electrons and where the second term is a Hartree-Fock (HF) approximation to this interaction which we use in constructing Φ_i^+. (More specifically, in constructing Φ_i^+, we describe the electron of the H atom by the $1s$ Coulomb function and the electrons of rare-gas atoms by ground-state HF wave functions. The radial wave functions describing the incident electron for each partial-wave contribution to Φ_i^+ are calculated in the appropriate term-dependent HF potential [24], as discussed below and as specified explicitly in the Appendix.) Omitted in Eq. (2) are corrections to our description of rare-gas atom targets by ground-state HF wave functions. Such corrections stem from electron correlations among the target electrons, as examined in more detail in Sec. II D below. We emphasize that our inclusion of $V_{\rm HF}^{N+1}$ in the description of the initial state is an improvement upon the typical description of the incident electron by a plane wave. In particular, it is needed to describe theoretically the experimentally observed target effects.

The final-state wave function Ψ_f^- in Eq. (1) should be in principle the exact solution to the full Hamiltonian satisfying the exact boundary conditions [25] for two continuum electrons moving in the Coulomb field of the ionized target. We have expanded our final-state wave function in independent electron states for the two continuum electrons and have coupled their orbital and spin angular momenta to partial waves characterized by L and S. These LS-coupled partial waves for the pair of ionized electrons couple to the singly ionized target ion differently for H, He, and the other rare gases.

For H, L and S are the total orbital and spin angular momenta of the system and are thus conserved during the collision. For He, the target ion is in a ^2S state and hence L is the total orbital angular momentum of the system. However, S must be coupled to the spin of the target electron to form the system's spin, which equals $\frac{1}{2}$. Thus, in He, the target electron couples singlet and triplet states of the continuum electron pair. However, we have ignored such interchannel coupling in the case of He and treat the channels designated by L and S as uncoupled. Finally, for Ne, Ar, Kr, and Xe, the target ion is in a ^2P state and neither L nor S is a good quantum number for the entire collision system. In general, there may be several LS partial waves of the continuum electron pair which may couple to the ^2P state of the target ion to form a particular total (T) orbital and spin angular momentum state $L_T S_T$ of the system. In our calculations for Ne, Ar, Kr, and Xe we have approximated the interchannel interactions between the set of partial waves LS which contribute to a given state $L_T S_T$ of the system by those interactions which are diagonal in L. These approximations used in calculating our final-state wave functions for rare-gas targets are defined explicitly in the Appendix.

A further approximation to Ψ_f^- in our calculations is our replacement of the exact Coulomb interaction between the two continuum electrons by a variationally determined screening potential [26–28]. For the configuration considered here in which $\hat{\mathbf{k}}_1=-\hat{\mathbf{k}}_2$, the effective charges Δ_1 and Δ_2 are determined by the condition [26–28]

$$-\frac{Z_T-\Delta_1}{k_1}-\frac{Z_T-\Delta_2}{k_2}=-\frac{Z_T}{k_1}-\frac{Z_T}{k_2}+\frac{1}{k_1+k_2}\ , \tag{3}$$

where Z_T is the net asymptotic charge of the ionized target. In our calculations we satisfy Eq. (3) using the following screening charges [28]:

$$\Delta_i\equiv\frac{k_i^2}{(k_1+k_2)^2}\quad (i=1,2)\ . \tag{4}$$

This choice of screening charges ensures that asymptotically each of the ionized electrons experiences the correct classical force (assuming that $\hat{\mathbf{r}}_1=\hat{\mathbf{k}}_1$, $\hat{\mathbf{r}}_2=\hat{\mathbf{k}}_2$, and $r_1/k_1=r_2/k_2$). It also ensures that the total potential energy for the system is correct at asymptotic distances.

In our calculations, these screening charges are used to replace the exact Coulomb interaction by the sum of the following screening potentials ($i=1,2$):

$$V_i(k_1,k_2)=\Delta_i y_0(r) \tag{5}$$

where $y_0(r)$ is chosen to have the properties that $y_0\to 0$ as $r\to 0$ and $y_0\to 1/r$ as $r\to\infty$. Specifically, $y_0(r)$ is a special case of the general function

$$y_\lambda(nl,n'l';r)\equiv r^{-(\lambda+1)}\int_0^r t^\lambda P_{nl}(t)P_{n'l'}(t)dt + r^\lambda\int_r^\infty t^{-(\lambda+1)}P_{nl}(t)P_{n'l'}(t)dt\ , \tag{6}$$

where $P_{nl}(r)$ is a radial wave function for the nl subshell of the target atom. If we denote the valence subshell of our target atom by n_0l_0, then $y_0(r)\equiv y_{\lambda=0}(n_0l_0,n_0l_0;r)$.

In what follows, we define explicitly our initial and final wave functions as well as the form of the T-matrix elements in our calculations. We then reduce the general triply differential cross section in Eq. (1) to forms specific to H, He, and other rare-gas targets in which dynamical and geometrical factors are clearly specified.

B. Partial-wave expansions

The initial state Φ_i^+ is characterized by the orbital and spin angular momenta of the N-electron target, denoted by $L_0M_0S_0M_{S_0}$, and by the momentum $\mathbf{k}$, and spin magnetic quantum number m_s of the incident electron. The final state Ψ_f^- is characterized by the orbital and spin angular momenta of the $(N-1)$-electron target ion core, denoted by $L_CM_CS_CM_{S_C}$, and by the momenta, $\mathbf{k}_1$ and $\mathbf{k}_2$, and spin magnetic quantum numbers, m_{s_1} and m_{s_2}, of the two continuum electrons. Since the Coulomb interactions which govern the $(e,2e)$ process are diagonal in the total orbital and spin angular momenta (denoted by $L_TM_TS_TM_{S_T}$) of the $(N+1)$-electron collision system, it is convenient to express the transition matrix amplitudes as a coherent sum of contributions characterized by the quantum numbers $L_TM_TS_TM_T$. This requires that we expand the continuum electron momentum states in partial waves in both initial and final states.

1. Single-electron wave functions

The partial-wave expansion for a single-electron wave function characterized asymptotically by momentum $\mathbf{k}$ and spin magnetic quantum number m_s is [29]

$$\phi^{(\pm)}_{\mathbf{k}m_s}(\mathbf{r})=k^{-1/2}\sum_{l=0}^{\infty}\sum_{m=-l}^{+l} i^l\exp[\pm i(\sigma_l+\delta_l)]Y^*_{lm}(\hat{\mathbf{k}}) \times r^{-1}P_{\varepsilon l}(r)Y_{lm}(\hat{\mathbf{r}})\chi_{m_S}\ . \tag{7}$$

In Eq. (7), the + and − superscripts on the one-electron wave function denote the outgoing wave and incoming wave boundary conditions that are appropriate, respectively, for the initial- and final-state continuum electrons [30]. The Y_{lm} functions in Eq. (7) are spherical harmonics and χ_{m_s} is a two-component spinor. The Coulomb phase σ_l is defined by [30]

$$\sigma_l\equiv\arg\Gamma(l+1-iq/k)\ , \tag{8}$$

where q is the net charge of the target atom or ion. Of course, if $q=0$, then $\sigma_l=0$. Note that for *final*-state continuum electrons, the net charge q includes the effect of electron screening [cf. Eqs. (3)–(5)]. The radial function has the asymptotic form

$$P_{\varepsilon l}(r)\underset{r\to\infty}{\sim}\left[\frac{2}{\pi k}\right]^{1/2}\sin[kr-l\pi/2+(q/k)\ln(2kr) +\sigma_l+\delta_l]\ , \tag{9}$$

where δ_l is the phase shift with respect to a Coulomb wave, or, if $q=0$, with respect to a plane wave. The phase shift carries information about the short-range interactions between the target atom or ion and the continuum electrons. In general, both the radial wave function $P_{\varepsilon l}(r)$ and its phase shift δ_l depend on both the state of the target atom or ion and on the angular momentum coupling of the continuum electron to the target atom or ion. These dependences will be displayed explicitly when we specify the initial and final states of the $(N+1)$-electron system. Finally, the momentum state wave function in Eq. (7) is normalized to a δ function in momentum $\mathbf{k}$, while the radial wave function in Eq. (9) is normalized to a δ function in energy ε, where $\varepsilon\equiv k^2/2$.

2. Initial-state wave function

Using a partial-wave expansion such as that in Eq. (7) for the incident electron, we may expand the initial state Φ_i^+ in terms of antisymmetrized, LS-coupled wave functions $\Psi_i((L_0l)L_TM_T(S_0\frac{1}{2})S_TM_{S_T})$ for the $(N+1)$-electron collision complex,

$$\Phi_i^+=k^{-1/2}\sum_{l=0}^{\infty}\sum_{m=-l}^{+l}\sum_{L_T,M_T}\sum_{S_T,M_{S_T}} i^l\exp[+i\delta_l(L_0S_0L_TS_T)]Y^*_{lm}(\hat{\mathbf{k}})\Psi_i((L_0l)L_TM_T(S_0\tfrac{1}{2})S_TM_{S_T}) \times\langle L_TM_T|L_0M_0lm\rangle\langle S_TM_{S_T}|S_0M_{S_0}\tfrac{1}{2}m_s\rangle\ , \tag{10}$$

ed, respectively, in the Hartree and in the HF approximations, as we demonstrate below when we present our numerical results. Additional treatment of capture processes requires a higher-order treatment of electron correlations within the target, which we formulate here.

Let us return to basics [23]. Our initial-state wave function $|\Phi_i^+\rangle$ is the solution of an approximate HF Hamiltonian,

$$H_i \equiv \sum_{i=1}^{N+1} [H_0(\mathbf{r}_i)+V_{\rm HF}(\mathbf{r}_i)] \ , \tag{20}$$

where $H_i|\Phi_i^+\rangle \equiv E_i|\Phi_i^+\rangle$, $H_0(\mathbf{r}_i)$ is the sum of kinetic energy and other radial potentials for the ith electron, and $V_{\rm HF}(\mathbf{r}_i)$ is the HF potential for the ith electron. In contrast, the exact Hamiltonian $H_{\rm exact}$ is

$$H_{\rm exact} \equiv \sum_{i=1}^{N+1} H_0(\mathbf{r}_i)+\sum_{j>i=1}^{N+1} \frac{1}{|\mathbf{r}_j-\mathbf{r}_i|} \ . \tag{21}$$

The difference between $H_{\rm exact}$ and H_i is

$$H_{\rm exact}-H_i = V+V' \tag{22}$$

where V is defined in Eq. (2) and where

$$V' = \sum_{j>i=1}^{N} \frac{1}{|\mathbf{r}_j-\mathbf{r}_i|} - \sum_{i=1}^{N} V_{\rm HF}(\mathbf{r}_i) \ . \tag{23}$$

In Eq. (1), our transition matrix element was approximated by assuming $V'=0$, i.e., that the target atom Hamiltonian for He, Ne, Ar, Kr, and Xe targets could be accurately described by the HF Hamiltonian. The exact treatment is to represent the transition matrix amplitude T_{fi} by,

$$T_{fi} = \langle \psi_{f({\rm exact})}^- | V+V' | \Phi_i^+ \rangle \ , \tag{24}$$

provided, of course, that ψ_f^- is indeed the *exact* final-state wave function. However, this formulation is troublesome for numerical calculations since matrix elements of V' may involve an overlap of the incident continuum electron with one of the final continuum electrons. (In our calculations, an initial continuum radial wave function is not necessarily orthogonal to a final continuum radial wave function since they are calculated using different potentials.)

Our Eq. (1), however, is exact for the *approximate* final-state wave function we employ. That is,

$$\langle \psi_{f({\rm approx})}^- | V' | \Phi_i^+ \rangle \equiv 0 \ . \tag{25}$$

This result stems from our use of the frozen-core approximation for the final-state target electrons as well as our use of a single Hermitian potential (cf. the Appendix) to describe both bound and continuum electrons in the final state. The well-known property [34] that matrix elements of the perturbation V' between frozen-core HF configurations that differ only by a single electron orbital wave function are zero then gives the result in Eq. (25). Two conclusions stem from the result in Eq. (25). First, to the extent that our description of the final state is a good approximation, target electron correlation effects on the $(e,2e)$ processes we study in this paper should be small. Second, in order to calculate the effect of target electron correlations on the $(e,2e)$ processes we study *without introducing a different representation of the final state,* we require an alternative formulation for the transition matrix amplitude T_{fi}.

For this reason, we define the state $|\chi_i^+\rangle$ as an eigenstate of the Hamiltonian H_i+V', i.e., $(H_i+V')|\chi_i^+\rangle = E_i|\chi_i^+\rangle$. It follows then that

$$T_{fi} = \langle \psi_f^- | V | \chi_i^+ \rangle \ , \tag{26}$$

where ψ_f^- should be the exact final-state wave function, but, of course, we plan later to substitute our approximate final-state wave function. Using now the formal representation of $|\chi_i^+\rangle$ in terms of $|\Phi_i^+\rangle$, i.e.,

$$|\chi_i^+\rangle \equiv |\Phi_i^+\rangle + \frac{1}{E_i-H_i+i\eta} V'|\chi_i^+\rangle \ , \tag{27}$$

we easily obtain an expansion of T_{fi} in powers of V':

$$T_{fi} = \langle \psi_f^- | V | \Phi_i^+ \rangle + \langle \psi_f^- \left| V \frac{1}{E_i-H_i+i\eta} V' \right| \Phi_i^+ \rangle + \cdots \ . \tag{28}$$

The second term in Eq. (28) represents a correction to the transition amplitude in our Eq. (1) stemming from electron correlation effects among the electrons of the target. Such corrections do not apply, of course, for H-atom targets. Among the processes represented by the second term in Eq. (28) are those in which V' promotes two target electrons to bound or continuum excited orbitals; the incident electron may then interact via V with one or the other of these two excited target electrons, possibly resulting in capture of the incident electron by the target.

We have treated some electronic correlations, including those explicitly leading to capture of the incident electron, stemming from the second term in Eq. (28) for the case of He targets. Our interest is in determining the magnitude of such higher-order effects relative to those stemming from the first term in Eq. (28). The explicit interactions we have treated are given in the Appendix. Our results are presented in the next section. As we expected, it turns out that for He the corrections stemming from the second term in Eq. (28) are small.

III. RESULTS

A. Symmetry properties of $\sigma^{(3)}$

Since all of our results concern the final-state configuration in which $\theta_{12}=\pi$ and since nearly all of our results presented in this paper concern the case in which the two continuum electrons share the available energy equally, it is useful to review the constraints which these special cases place on the triply differential cross sections [14,15]. First, since $\hat{\mathbf{k}}_1=-\hat{\mathbf{k}}_2$, the $3j$ symbol originating from the right-hand side of Eq. (12) implies that the amplitude A in Eq. (15) is nonzero if and only if $(-1)^L=(-1)^{l_1+l_2}$. Thus only those angular momenta L of the final-state continuum electron pair are permitted

for $3j$ symbols may then be used to collapse the double sum over pairs of spherical harmonics (dependent on the arguments $\hat{\mathbf{k}}_1$ and $\hat{\mathbf{k}}$) into a single sum, which may be expressed in terms of Legendre polynomials (dependent on the argument $\hat{\mathbf{k}}_1\cdot\hat{\mathbf{k}}$) using a standard relationship [33].

The result is that the triply differential cross section in Eq. (13) summed over final states and averaged over initial states may be written as follows:

$$\sigma^{(3)}\equiv([L_0][S_0][\tfrac{1}{2}])^{-1}\sum_{M_0,M_{S_0},m_S}\sum_{m_{s_1},m_{s_2},M_{S_C},M_C}\frac{d^3\sigma}{d\varepsilon_2 d\Omega_1 d\Omega_2}$$

$$=\frac{\pi}{4k^2[L_0]}\sum_{L_T,L_T'}\sum_{L,L'}\sum_{l,l'}\sum_{S,S_T}A(l,L,S,L_T,S_T)A^*(l',L',S,L_T',S_T)$$

$$\times\sum_{\lambda}[\lambda]P_\lambda(\hat{\mathbf{k}}_1\cdot\hat{\mathbf{k}})(-1)^{L_C+L_0}[L_T][L_T'](L][L'][l][l'])^{1/2}$$

$$\times\begin{bmatrix}L & L' & \lambda\\ 0 & 0 & 0\end{bmatrix}\begin{bmatrix}l & l' & \lambda\\ 0 & 0 & 0\end{bmatrix}\begin{Bmatrix}L_T & L_T' & \lambda\\ L' & L & L_C\end{Bmatrix}\begin{Bmatrix}L_T & L_T' & \lambda\\ l' & l & L_0\end{Bmatrix}. \tag{14}$$

In Eq. (14), the symbol $[x]\equiv 2x+1$ and the amplitudes A are defined by

$$A(l,L,S,L_T,S_T)\equiv\left[\frac{[S_T]}{2[S_0]}\right]^{1/2}\sum_{l_1,l_2}(-1)^{l_1+L}f(l,l_1,l_2)([l_1][l_2])^{1/2}\begin{bmatrix}l_1 & l_2 & L\\ 0 & 0 & 0\end{bmatrix}$$

$$\times\langle\Psi_f([L_C(l_1l_2)L]L_T[S_C(\tfrac{1}{2}\tfrac{1}{2})S]S_T)|V|\Psi_i((L_0l)L_T(S_0\tfrac{1}{2})S_T)\rangle \tag{15}$$

where

$$f(l,l_1,l_2)\equiv i^{l+l_1+l_2}\exp[i(\delta_l+\sigma_{l_1}+\delta_{l_1}+\sigma_{l_2}+\delta_{l_2})]\ . \tag{16}$$

The general expression for $\sigma^{(3)}$ in Eq. (14) simplifies further for the cases of interest in this paper. Thus, for the H atom, $L_0=L_C=S_C=0$, $L=l=L_T$, $L'=l'=L_T'$, and $S_T=S$. Hence Eq (14) becomes

$$\sigma_{\rm H}^{(3)}=\frac{\pi}{4k^2}\sum_{L,L'}\sum_{S}A_{\rm H}(LS)A_{\rm H}^*(L'S)\sum_{\lambda}[\lambda]P_\lambda(\hat{\mathbf{k}}_1\cdot\hat{\mathbf{k}})[L][L']\begin{bmatrix}L & L' & \lambda\\ 0 & 0 & 0\end{bmatrix}^2. \tag{17}$$

For rare-gas (RG) atom targets, $L_0=S_0=0$, $S_T=S_C=\frac{1}{2}$, $L_T=l$, and $L_T'=l'$. Hence Eq. (14) becomes

$$\sigma_{\rm RG}^{(3)}=\frac{\pi}{4k^2}\sum_{L,L'}\sum_{S}\sum_{l,l'}A_{\rm RG}(lLS)A_{\rm RG}^*(l'L'S)\sum_{\lambda}[\lambda]P_\lambda(\hat{\mathbf{k}}_1\cdot\hat{\mathbf{k}})(-1)^{L_C}[l][l'](L][L'])^{1/2}$$

$$\times\begin{bmatrix}L & L' & \lambda\\ 0 & 0 & 0\end{bmatrix}\begin{bmatrix}l & l' & \lambda\\ 0 & 0 & 0\end{bmatrix}\begin{Bmatrix}l & l' & \lambda\\ L' & L & L_C\end{Bmatrix}. \tag{18}$$

Finally, for the He atom, Eq. (18) reduces further since $L_C=0$, $l=L$, and $l'=L'$. Hence Eq. (18) becomes

$$\sigma_{\rm He}^{(3)}=\frac{\pi}{4k^2}\sum_{L,L'}\sum_{S}A_{\rm He}(LS)A_{\rm He}^*(L'S)$$

$$\times\sum_{\lambda}[\lambda]P_\lambda(\hat{\mathbf{k}}_1\cdot\hat{\mathbf{k}})[L][L']$$

$$\times\begin{bmatrix}L & L' & \lambda\\ 0 & 0 & 0\end{bmatrix}^2. \tag{19}$$

Note that Eq. (19) is identical in form to Eq. (17) for the H atom. This has been achieved by including certain spin-dependent factors in our definition of the amplitudes in Eq. (15), i.e., those before the sum on the right-hand side. Explicit expressions for the amplitudes $A_{\rm H}$, $A_{\rm He}$, and $A_{\rm RG}$ are given in the Appendix.

D. Higher-order capture corrections

At first glance, our formulation of $(e,2e)$ processes in Eqs. (1) and (2) would appear to omit capture processes in which the incident electron not only ionizes a target electron but also exchanges places with a second target electron. Such processes involve a change of state of three one-electron orbitals. Since the transition operator V in Eq. (1) and (2) is a two-body operator, it cannot effect such a three-body transition. Nevertheless, capture processes are included *implicitly* in our formulation since the wave function of our incident electron is calculated in HF approximation in which exchange interactions with the target are included. Thus, while capture processes are not calculated *explicitly* in Eqs. (1) and (2), their *implicit* effects can be extracted by comparing results in which the radial wave function for the incident electron is calculat-

ed, respectively, in the Hartree and in the HF approximations, as we demonstrate below when we present our numerical results. Additional treatment of capture processes requires a higher-order treatment of electron correlations within the target, which we formulate here.

Let us return to basics [23]. Our initial-state wave function $|\Phi_i^+\rangle$ is the solution of an approximate HF Hamiltonian,

$$H_i \equiv \sum_{i=1}^{N+1} [H_0(\mathbf{r}_i)+V_{\rm HF}(\mathbf{r}_i)] \ , \tag{20}$$

where $H_i|\Phi_i^+\rangle \equiv E_i|\Phi_i^+\rangle$, $H_0(\mathbf{r}_i)$ is the sum of kinetic energy and other radial potentials for the ith electron, and $V_{\rm HF}(\mathbf{r}_i)$ is the HF potential for the ith electron. In contrast, the exact Hamiltonian $H_{\rm exact}$ is

$$H_{\rm exact} \equiv \sum_{i=1}^{N+1} H_0(\mathbf{r}_i) + \sum_{j>i=1}^{N+1} \frac{1}{|\mathbf{r}_j-\mathbf{r}_i|} \ . \tag{21}$$

The difference between $H_{\rm exact}$ and H_i is

$$H_{\rm exact}-H_i = V+V' \tag{22}$$

where V is defined in Eq. (2) and where

$$V' = \sum_{j>i=1}^{N} \frac{1}{|\mathbf{r}_j-\mathbf{r}_i|} - \sum_{i=1}^{N} V_{\rm HF}(\mathbf{r}_i) \ . \tag{23}$$

In Eq. (1), our transition matrix element was approximated by assuming $V'=0$, i.e., that the target atom Hamiltonian for He, Ne, Ar, Kr, and Xe targets could be accurately described by the HF Hamiltonian. The exact treatment is to represent the transition matrix amplitude T_{fi} by,

$$T_{fi} = \langle \psi_{f({\rm exact})}^- | V+V' | \Phi_i^+ \rangle \ , \tag{24}$$

provided, of course, that ψ_f^- is indeed the *exact* final-state wave function. However, this formulation is troublesome for numerical calculations since matrix elements of V' may involve an overlap of the incident continuum electron with one of the final continuum electrons. (In our calculations, an initial continuum radial wave function is not necessarily orthogonal to a final continuum radial wave function since they are calculated using different potentials.)

Our Eq. (1), however, is exact for the *approximate* final-state wave function we employ. That is,

$$\langle \psi_{f({\rm approx})}^- | V' | \Phi_i^+ \rangle \equiv 0 \ . \tag{25}$$

This result stems from our use of the frozen-core approximation for the final-state target electrons as well as our use of a single Hermitian potential (cf. the Appendix) to describe both bound and continuum electrons in the final state. The well-known property [34] that matrix elements of the perturbation V' between frozen-core HF configurations that differ only by a single electron orbital wave function are zero then gives the result in Eq. (25). Two conclusions stem from the result in Eq. (25). First, to the extent that our description of the final state is a good approximation, target electron correlation effects on the $(e,2e)$ processes we study in this paper should be small. Second, in order to calculate the effect of target electron correlations on the $(e,2e)$ processes we study *without introducing a different representation of the final state,* we require an alternative formulation for the transition matrix amplitude T_{fi}.

For this reason, we define the state $|\chi_i^+\rangle$ as an eigenstate of the Hamiltonian H_i+V', i.e., $(H_i+V')|\chi_i^+\rangle = E_i|\chi_i^+\rangle$. It follows then that

$$T_{fi} = \langle \psi_f^- | V | \chi_i^+ \rangle \ , \tag{26}$$

where ψ_f^- should be the exact final-state wave function, but, of course, we plan later to substitute our approximate final-state wave function. Using now the formal representation of $|\chi_i^+\rangle$ in terms of $|\Phi_i^+\rangle$, i.e.,

$$|\chi_i^+\rangle \equiv |\Phi_i^+\rangle + \frac{1}{E_i-H_i+i\eta} V' |\chi_i^+\rangle \ , \tag{27}$$

we easily obtain an expansion of T_{fi} in powers of V':

$$T_{fi} = \langle \psi_f^- | V | \Phi_i^+ \rangle + \langle \psi_f^- \left| V \frac{1}{E_i-H_i+i\eta} V' \right| \Phi_i^+ \rangle + \cdots \ . \tag{28}$$

The second term in Eq. (28) represents a correction to the transition amplitude in our Eq. (1) stemming from electron correlation effects among the electrons of the target. Such corrections do not apply, of course, for H-atom targets. Among the processes represented by the second term in Eq. (28) are those in which V' promotes two target electrons to bound or continuum excited orbitals; the incident electron may then interact via V with one or the other of these two excited target electrons, possibly resulting in capture of the incident electron by the target.

We have treated some electronic correlations, including those explicitly leading to capture of the incident electron, stemming from the second term in Eq. (28) for the case of He targets. Our interest is in determining the magnitude of such higher-order effects relative to those stemming from the first term in Eq. (28). The explicit interactions we have treated are given in the Appendix. Our results are presented in the next section. As we expected, it turns out that for He the corrections stemming from the second term in Eq. (28) are small.

III. RESULTS

A. Symmetry properties of $\sigma^{(3)}$

Since all of our results concern the final-state configuration in which $\theta_{12}=\pi$ and since nearly all of our results presented in this paper concern the case in which the two continuum electrons share the available energy equally, it is useful to review the constraints which these special cases place on the triply differential cross sections [14,15]. First, since $\hat{\mathbf{k}}_1=-\hat{\mathbf{k}}_2$, the $3j$ symbol originating from the right-hand side of Eq. (12) implies that the amplitude A in Eq. (15) is nonzero if and only if $(-1)^L=(-1)^{l_1+l_2}$. Thus only those angular momenta L of the final-state continuum electron pair are permitted

which have the same parity as the continuum electron pair.

Second, for the case of equal energy sharing, very general considerations [14,15] of the symmetry of the final-state wave function under interchange of the coordinates of the two continuum electrons leads to the result that the total spin S of the continuum electron pair must have the same parity as $(-1)^{l_1+l_2}$. That this same result follows for the particular multielectron final-state wave functions we employ in this paper may be seen by a detailed examination of the properties of the amplitudes A defined in Eq. (15). One may easily show that appropriate combinations of direct and exchange terms for the final-state pair $(\varepsilon_1 l_1, \varepsilon_2 l_2)$ with those for the exchange and direct terms, respectively, for the final-state pair $(\varepsilon_1 l_2, \varepsilon_2 l_1)$ lead (in the case that $\varepsilon_1 = \varepsilon_2$) to an overall factor $[1+(-1)^{L+S}]$ in the expressions for the amplitudes A.

The consequence of these symmetry properties of the transition amplitudes A on the triply differential cross section in Eq. (14) is as follows. Notice that both the amplitude A and its complex conjugate A^* in Eq. (14) depend on the same spin S for the final-state continuum electron pair. (This is a consequence of the summations over spin magnetic quantum numbers.) For the case of equal energy sharing, the amplitudes A and A^* are nonzero only if L and L' both have the same parity as S. This fact in turn implies that only Legendre polynomials P_λ having *even* values of λ contribute to Eq. (14) since the $3j$ symbol involving L, L', and λ in that equation is zero for *odd* values of λ.

Hence, when $\varepsilon_1 = \varepsilon_2$ for the case that $\theta_{12} = \pi$, the triply differential cross section is symmetric about $\theta_1 = \pi/2$ (if $\hat{\mathbf{k}}$ defines the z axis). Conversely, when $\varepsilon_1 \neq \varepsilon_2$, L and L' in Eq. (14) may have opposite parity. Thus Legendre polynomials with *odd* order λ contribute, leading to a loss of symmetry about $\theta_1 = \pi/2$.

B. Results for H and He targets

In Ref. [17] we presented triply differential cross-section results for $(e,2e)$ processes involving H and He targets for the cases in which the two final-state continuum electrons share 4 eV of excess energy. Both equal-energy-sharing ($\varepsilon_1 = \varepsilon_2 = 2$ eV) and unequal-energy-sharing ($\varepsilon_1 = 3.5$ eV and $\varepsilon_2 = 0.5$ eV) results were presented. In particular, a detailed analysis of the scattering amplitudes for the equal-energy-sharing case was presented in order to provide an explanation for the experimentally observed [6] target dependence of the $(e,2e)$ angular distributions for H and for He.

In this paper, we present first a detailed analysis of the unequal-energy-sharing case $\varepsilon_1 = 3.5$ eV and $\varepsilon_2 = 0.5$ eV, whose triply differential cross sections we presented in Ref. [17]. We then compare our $(e,2e)$ results with available experimental and other theoretical work for the cases of equal energy sharing of 2 eV and 0.5 eV excess energy. Finally, we exhibit the effect of exchange and of higher-order capture processes on our results.

1. Results for 4 eV excess energy with $\varepsilon_1 = 3.5$ eV and $\varepsilon_2 = 0.5$ eV

Our triply differential cross sections for this case are presented in Fig. 2 of Ref. [17]. The key features of these cross sections for H and for He may be understood from examination of our calculated amplitudes, which are presented in Table I. The relative magnitudes and phases of these amplitudes are shown for the first six partial waves L (for both $S=0$ and 1) of the final-state pair of continuum energy electrons. While the absolute magnitudes of these amplitudes are quite different for H and for He, the relative magnitudes of these amplitudes, which determine the angular distribution, are quite similar. Furthermore, the relative amplitudes for partial waves satisfying $(-1)^{L+S} = +1$ (which are the only ones that are allowed in the equal-energy-sharing case) are quite similar to those calculated for 4 eV excess energy with $\varepsilon_1 = \varepsilon_2 = 2$ eV (cf. Table I of Ref. [17]).

One observes from Table I that the same amplitudes which are dominant for the equal-energy-sharing case are also dominant for the unequal-energy-sharing case: namely, those amplitudes having $(-1)^{L+S} = +1$ with $L \leq 3$. The amplitudes having $(-1)^{L+S} = -1$ are an or-

TABLE I. Relative amplitude and phase for the electron-impact ionization scattering amplitudes $A(LS)$ for H and for He targets for final-state electron kinetic energies $\frac{1}{2}k_1^2 = 3.5$ eV and $\frac{1}{2}k_2^2 = 0.5$ eV.

	Relative amplitude $\lvert A(LS)\rvert / \lvert A(^1S^e)\rvert$				Arg $A(LS)$ (rad)			
	H $(-1)^{L+S}$		He $(-1)^{L+S}$		H $(-1)^{L+S}$		He $(-1)^{L+S}$	
Partial wave L	$+1$	-1	$+1$	-1	$+1$	-1	$+1$	-1
0	1.000[a]	0.052	1.000[a]	0.075	4.69[b]	1.87[b]	6.29	2.70
1	0.401	0.041	0.430	0.090	2.96	1.41	3.19	0.53
2	0.469	0.074	0.538	0.050	4.14	3.33	4.41	3.85
3	0.293	0.145	0.203	0.124	3.24	5.16	3.19	5.18
4	0.022	0.121	0.021	0.066	4.23	4.14	3.97	4.01
5	0.033	0.018	0.013	0.011	4.03	4.37	3.78	4.22

[a]For H, $\lvert A(^1S^e)\rvert = 0.3175$ a.u.; for He, $\lvert A(^1S^e)\rvert = 0.1943$ a.u.

[b]To facilitate comparison of H with He, all H amplitudes in this column have been multiplied by the phase $(-1)^{1+S}$ [cf. Eqs. (A13) and (A14)]. This was also done in Table I of Ref. [17].

der of magnitude smaller than those for $(-1)^{L+S}=+1$ for $L \leq 2$. Nevertheless, their presence enables Legendre polynomials of odd order to contribute to the triply differential cross section, thereby destroying the symmetry of the angular distribution about $\theta_1=\pi/2$ that one observes in the equal-energy-sharing case. The amplitudes with $(-1)^{L+S}=-1$ dominate those with $(-1)^{L+S}=+1$ only for $L \geq 4$; however, for these partial waves the amplitudes are an order of magnitude smaller than those for $L \leq 3$ and thus do not determine the broad features of the angular distribution.

As was found for the equal-energy-sharing case, the major difference between H and He in our calculations for the unequal-energy-sharing case is between the arguments of the $^1S^e$ partial-wave amplitudes, which differ by more than 1.6 rad. This difference affects the triply differential cross sections in Eqs. (17) and (19) primarily via the interference terms between the $L=0$ and 2 partial waves, which contribute to the coefficient of the $\lambda=2$ Legendre polynomial. These interference terms in H and in He have phases which differ by more than 1.3 rad. As noted in Ref. [17], it is this phase difference between H and He for the sum $A(^1S^e)A^*(^1D^e)+A(^1D^e)A^*(^1S^e)$ which largely explains the observed target effects of the $(e,2e)$ triply differential cross section.

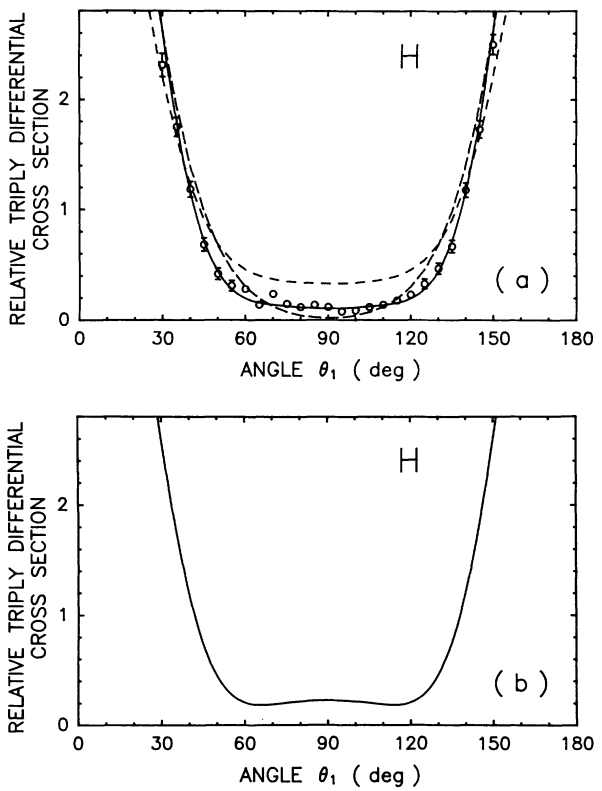

FIG. 1. Relative triply differential $(e,2e)$ cross sections for a H atom target for final states having $\theta_{12}=\pi$ and the continuum electrons sharing the excess energy E_{ex} equally. (a) $E_{ex}=2$ eV, (b) $E_{ex}=0.5$ eV. Solid line: present theoretical results [cf. Eqs. (29) and (17)]. Open circles: experimental results of Rösel, Bär, Jung, and Ehrhardt, Ref. [35]. Long-dashed curve: theoretical results of Brauner *et al.*, Ref. [16]. Short-dashed curve: theoretical results of Jones, Madison, and Srivastava, Ref. [18].

Note finally that in the unequal-energy-sharing case, whose amplitudes are presented in Table I, the $^1P^o$ amplitudes for H and for He also have a large phase difference of nearly 0.9 rad. However, as noted already, the relative amplitudes of these partial waves are an order of magnitude smaller than the dominant amplitudes having $(-1)^{L+S}=+1$. Thus the effect of the large phase difference for the $^1P^o$ amplitudes is of far less importance than that for the $^1S^e$ amplitudes in explaining the experimentally observed target effects. Indeed, when we perform the numerical experiment of replacing the He $^1P^o$ amplitude's phase by that for H we find that the local maximum in the relative cross section at $\theta_1=\pi/2$ is almost unchanged in magnitude. Only the magnitudes of the local minima at $\theta_1=50°$ and 130° as well as rates of increase at low and at high angles change noticeably.

2. *Results for 2 eV and 0.5 eV excess energy with equal energy sharing*

Our results for the case in which the two final-state electrons share equally 2 and 0.5 eV excess kinetic energy are shown in Fig. 1 for a H-atom target and in Fig. 2 for

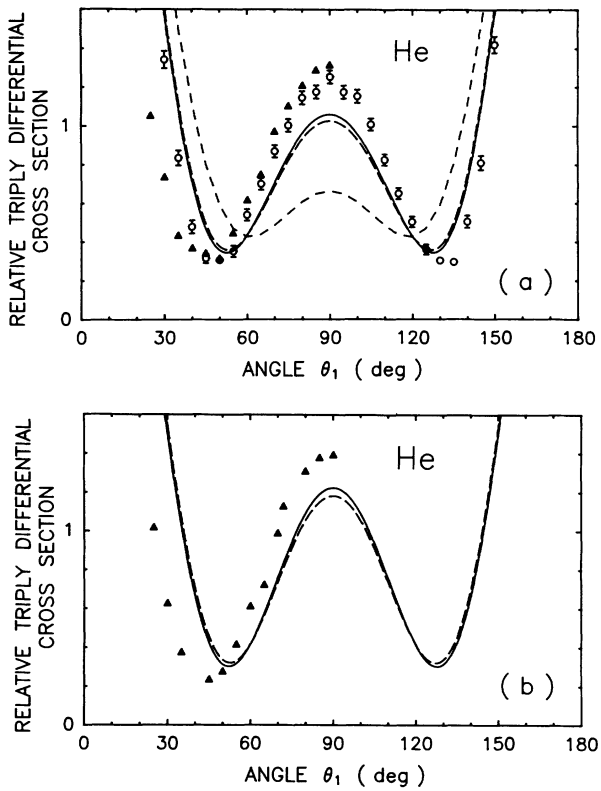

FIG. 2. Relative triply differential $(e,2e)$ cross sections for a He-atom target for final states having $\theta_{12}=\pi$ and the continuum electrons sharing the excess energy E_{ex} equally. (a) $E_{ex}=2$ eV, (b) $E_{ex}=0.5$ eV. Solid line: present theoretical results [cf. Eqs. (29) and (19)]. Long-dashed line: present theoretical results including higher-order capture corrections (cf. text, Sec. II D). Short-dashed curve: theoretical results of Jones, Madison and Srivastava, Ref. [18]. Open circles: experimental results of Rösel, Bär, Jung, and Ehrhardt, Ref. [20]. Solid triangles: experimental results of Selles, Huetz, and Mazeau, Ref. [5].

a He-atom target. Since the experimental data are relative, we plot the relative triply differential cross sections

$$\frac{4\pi}{\sigma}\sigma^{(3)}=1+\sum_{\lambda>0}\beta_\lambda P_\lambda(\hat{\mathbf{k}}_1\cdot\hat{\mathbf{k}}) \tag{29}$$

where σ and β_λ are defined by comparison of Eq. (29) with Eq. (17) in the case of H and with Eq. (19) in the case of He. The relative experimental data were fit to our results using Eq. (29) and a standard least-squares procedure which takes account of the experimental error estimates.

Figure 1(a) shows that our theoretical results for the case of 2 eV excess energy are in excellent agreement with the experimental measurements of Rösel *et al.* [35]. Since these relative experimental measurements have been fit to our calculated results, the comparisons with the theoretical calculations of Brauner *et al.* [16] and with Jones, Madison, and Srivastava [18] are shown at a disadvantage. However, even when fits of experiment to these other theoretical results [16,18] are carried out, the remaining discrepancies between these other theoretical results [16,18] and experiment [35] are qualitatively similar to those between our calculation and these other theoretical results. Namely, our calculations predict a higher and flatter cross section in the vicinity of 90° than do those of Brauner *et al.* [16]. Furthermore, the width in θ_1 of the bottom of the bowl-shaped cross section is predicted to be somewhat wider in our calculations than in those of Brauner *et al.* [16]. However, our cross sections are significantly lower in magnitude in the range $40°\lesssim\theta_1\lesssim 140°$ than those of Jones, Madison, and Srivastava [18].

Although the theoretical results of Brauner *et al.* [16], Jones, Madison, and Srivastava [18], and ours more or less agree qualitatively for the relative triply differential cross section for H shown in Fig. 1(a), there are significant quantitative discrepancies for the absolute values of $\sigma^{(3)}$. Since these differences depend on the angle θ_1, we present in Table II the values of σ which we have calculated by integrating each group's results for $\sigma^{(3)}$ over the solid angle Ω_1 [cf. Eq. (29)] for the case $\varepsilon_1=\varepsilon_2=1$ eV and $\theta_{12}=\pi$. One sees that the result of Brauner *et al.* [16] for σ is two orders of magnitude smaller than those of either Jones, Madison, and Srivastava [18] or ours, as has been noted already in Ref. [18]. Brauner *et al.* [16] have attributed the small values of their absolute results near threshold to the wave-function normalization they used. The result of Jones, Madison, and Srivastava [18] and ours are of the same order of magnitude, but ours is slightly larger.

Figure 1(b) shows our theoretical results for the case of 0.5 eV excess energy. These results are interesting because there is a small but noticeable local maximum at $\theta_1=\pi/2$. Our calculations for $E_{ex}\geq 1.0$ eV (not all of which are shown) all give a minimum of $\sigma_H^{(3)}$ at $\theta_1=\pi/2$. No experimental data for 0.5 eV excess energy are known to us.

Figure 2(a) shows our theoretical results for He for the case of $E_{ex}=2$ eV. We present two of our theoretical results: one with (long-dashed curve) and one without (solid curve) inclusion of the higher-order capture processes mentioned in Sec. II D above and discussed in more detail below. Clearly such processes have only a very small effect (primarily in reducing slightly the height of the local maximum at $\theta_1=\pi/2$), thereby indicating that our approximations are consistent, as discussed in Sec. II D. Both of our results are in qualitative agreement with the relative experimental measurements of Selles, Huetz, and Mazeau [5] and of Rösel *et al.* [20]. The short-dashed curve represents the theoretical results of Jones, Madison, and Srivastava [18], which predict a much lower maximum at $\theta_1=\pi/2$ than found either by us or by experiment [5,20]. Comparisons of the absolute values of σ for He are presented in Table II. Our result appears to be a factor of 2 or so higher than that of Jones, Madison, and Srivastava [18]. Clearly, absolute experimental measurements of $\sigma^{(3)}$ are needed to resolve this disagreement for He (as well as the disagreements mentioned above for H).

In Fig. 2(b) our theoretical results with and without inclusion of higher-order capture processes are presented for the case of $E_{ex}=0.5$ eV. Again, there is qualitative agreement with the relative experimental measurements of Selles, Huetz, and Mazeau [5].

3. *Analysis of exchange and capture effects*

When one formulates the $(e,2e)$ process in a basis of states in which the incident electron is not antisymmetrized with respect to the target electrons (cf., e.g., Refs. [3,18,26], the effects of exchange and capture can be easily presented as these effects require separate calcula-

TABLE II. Absolute integrated triply differential cross section σ for H and He for the case $\theta_{12}=\pi$ and $\frac{1}{2}k_1^2=\frac{1}{2}k_2^2=1$ eV.

	σ (a.u.)[a]		
Target	Brauner *et al.*[b]	Jones, Madison, and Srivastava[c]	Present results
H	0.0135	3.19	3.73
He		0.358	0.762

[a]From Eq. (29), $\sigma=\int_0^{2\pi}d\phi_1\int_{-1}^{+1}\sigma^{(3)}d(\cos\theta_1)$.
[b]Calculated from data for $\sigma^{(3)}$ presented in Ref. [16], Fig. 6.
[c]Calculated from data for $\sigma^{(3)}$ presented in Ref. [18], Fig. 5.

tions. In our calculations, however, all initial and final states are explicitly antisymmetrized and, in fact, exchange interactions are taken into account in calculating the continuum electrons' radial wave functions. Thus effects of exchange and capture processes are implicit in our calculations. Nevertheless, we can examine their effects by doing numerical experiments in which some of these exchange effects are selectively turned off (i.e., not included). The results of these numerical experiments are presented in Fig. 3, whose results we now discuss.

Our procedure of treating exchange interactions between the continuum electrons and any electrons in the target atom or ion includes implicitly a treatment of capture. However, since we treat exchange effects to infinite order, we cannot determine if the incident electron, for example, remains behind on the target ion, or whether, after some indeterminate number of exchanges, it escapes as one of the final continuum electrons. However, by turning off such exchange interactions we can obtain a clear picture of the numerical effect of such exchange interactions and thereby also a crude estimate of the magnitude of capture processes.

The results of such numerical experiments are shown in Fig. 3. We see immediately that the effect of exchange in both H and He is primarily to affect the magnitudes of the cross sections near $\theta_1=\pi/2$, but not to change their qualitative shapes. In H, omitting exchange in calculating the radial wave functions of the incident electron tends to raise the magnitude of the cross-section minimum at $\theta_1=\pi/2$. In He, omission of exchange in calculating the radial wave functions of the incident electron tends in contrast to lower the magnitude of the cross-section maximum at $\theta_1=\pi/2$. For He, when exchange is omitted also in calculating the radial wave functions for the final-state continuum electrons, the local maximum is lowered even further. (In H, of course, the final state does not have any target electrons with which the continuum electrons can undergo exchange.)

Consider now the higher-order capture processes we discussed in Sec. II D above. Our results including such effects by means of the second term in Eq. (28) are shown for He targets as the long-dashed curve in Fig. 2. We have not done numerical experiments in which such higher-order corrections are calculated without inclusion of exchange since their overall effects are so small (cf. Fig. 2).

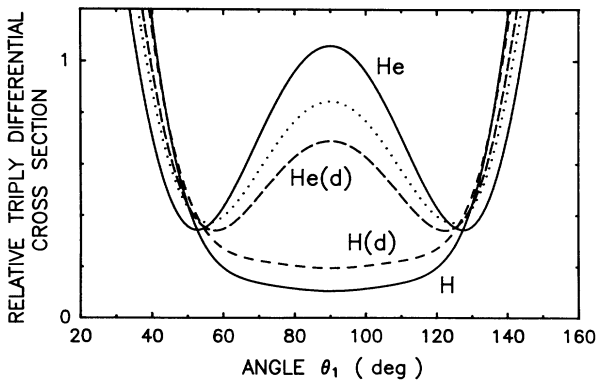

FIG. 3. Relative triply differential $(e,2e)$ cross sections for H and He targets for the case of 2 eV excess energy with equal energy sharing. Solid curves: present theoretical results including all exchange interactions. Dashed curves: present theoretical results omitting all exchange interactions, designated H(d) and He(d). Dotted curve: present theoretical results for He omitting only exchange interactions of the incident electron with the target electrons.

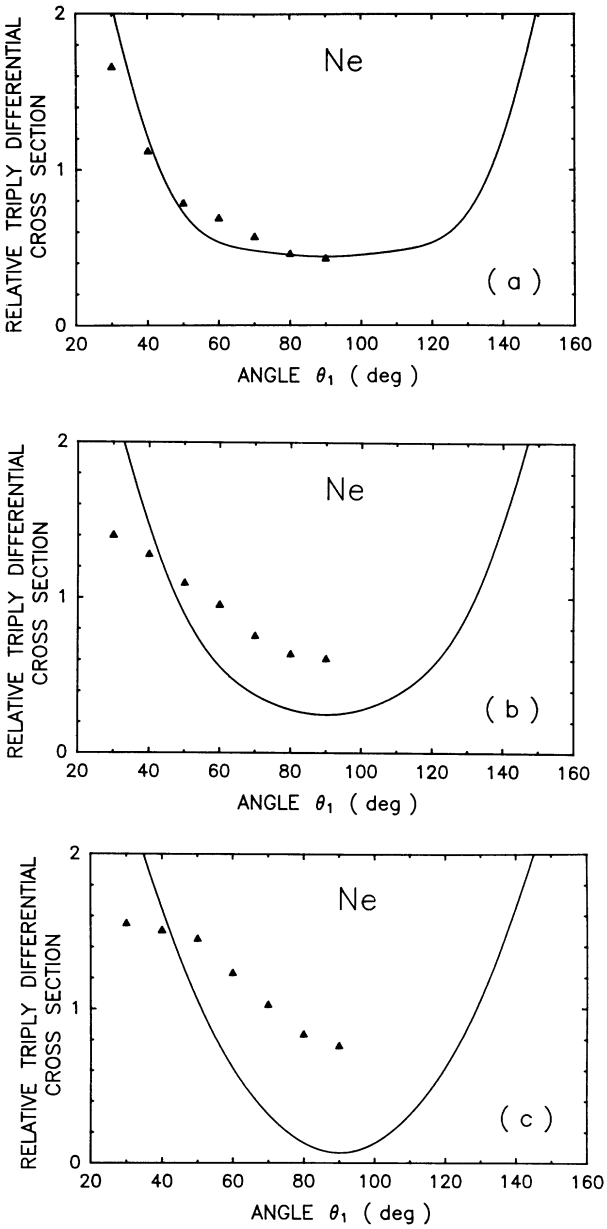

FIG. 4. Relative triply differential $(e,2e)$ cross sections for a Ne-atom target for final states having $\theta_{12}=\pi$ and the continuum electrons sharing the excess energy E_{ex} equally. (a) $E_{ex}=4$ eV, (b) $E_{ex}=2$ eV, (c) $E_{ex}=0.5$ eV. Solid curves: present theoretical results [cf. Eqs. (29) and (18)]. Solid triangles: experimental results of Selles, Mazeau, and Huetz (Ref. [8]).

Our conclusion regarding capture processes on the $(e,2e)$ triply differential cross sections for H and for He is that such effects may be quantitatively significant. However, they do not explain the qualitative differences in the angular distributions for H and for He. (This conclusion is reached also by Jones, Madison, and Srivastava [18].) Rather, the qualitative differences stem from other short-range (specifically, direct potential) effects on the s-wave phase shifts of both incident and final-state continuum electrons [17].

C. Results for Ne, Ar, Kr, and Xe targets

As noted in Sec. II A, our calculations for the heavier rare-gas targets are more approximate than those for either H or He targets. The reason is that the heavier rare-gas target ions in the final state have angular momentum $L_C=1$ rather than $L_C=0$. This nonzero angular momentum means that the angular momentum L of the final continuum electron pair is no longer a good quantum number for the final state. We have approximated the final-state interchannel interactions between different angular momenta L (for fixed total angular momentum L_T for the final state) by retaining only those interactions which are explicitly diagonal in L. This approximation is defined more precisely in the Appendix. What we have retained is a substantial portion of the intrachannel interactions of each LS state of the final continuum electron pair with the residual target ion.

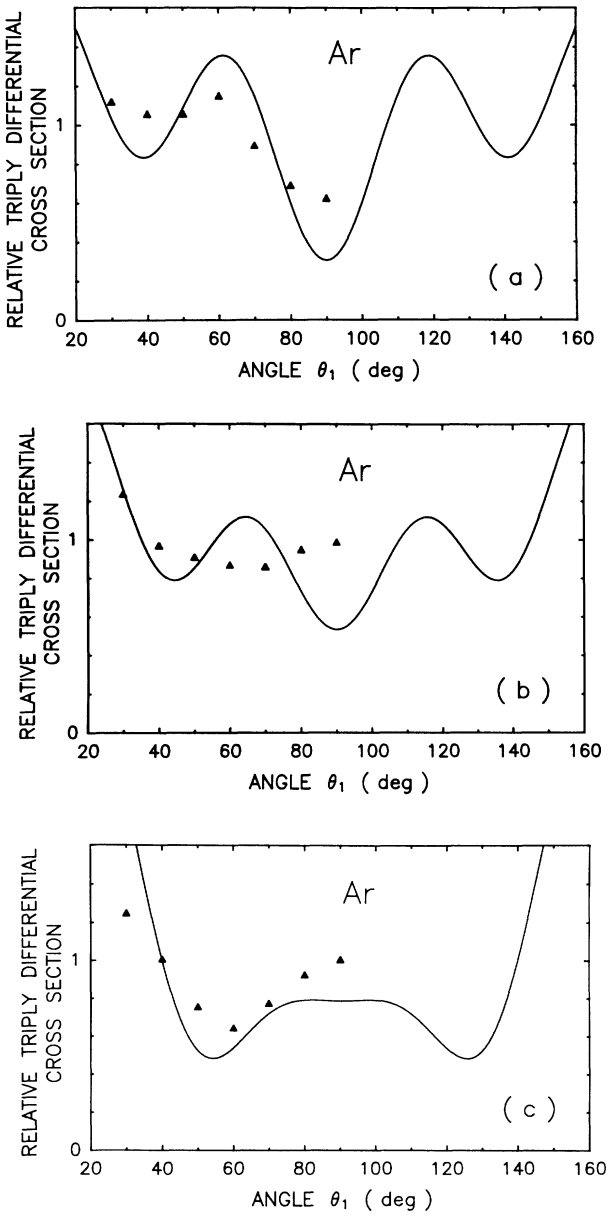

FIG. 5. Same as for Fig. 4 for an Ar-atom target.

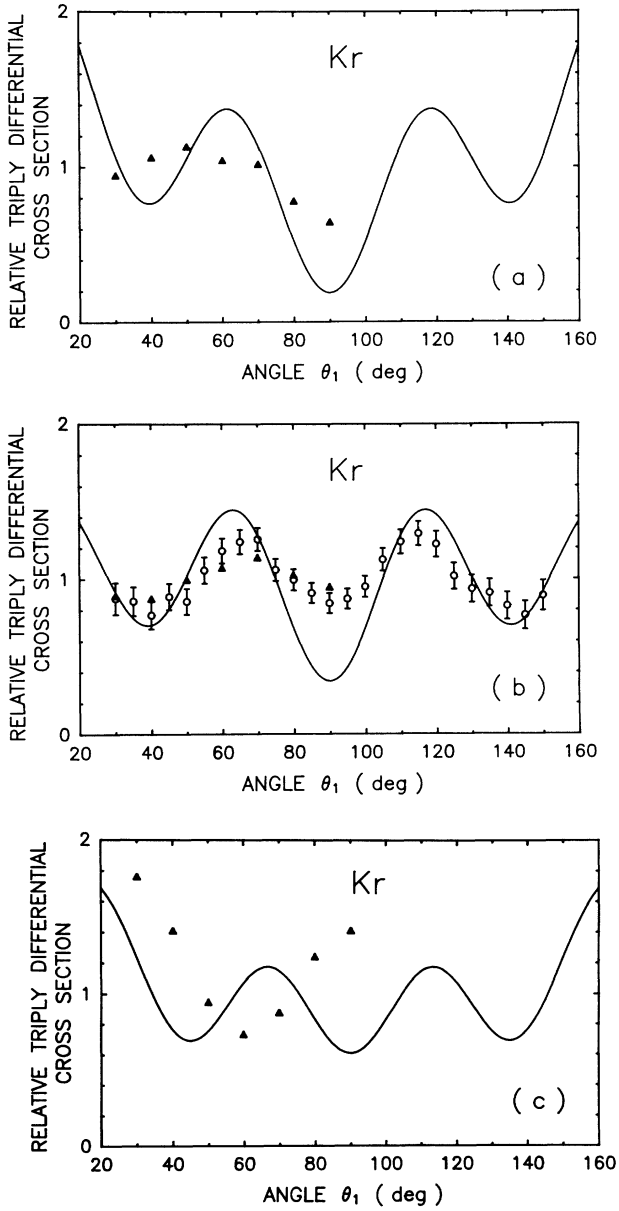

FIG. 6. Same as for Fig. 4 for a Kr-atom target, with the following addition: the open circles are experimental results of Rösel, Bär, Jung, and Ehrhardt, Ref. [7].

TABLE III. Dynamical parameters determining the absolute triply differential cross section $\sigma^{(3)}$ for the case $\theta_{12}=\pi$ and $\frac{1}{2}k_1^2=\frac{1}{2}k_2^2=1$ eV.

Parameter[a]	Target					
	H	He	Ne	Ar	Kr	Xe
σ (a.u.)	3.73	0.762[b]	0.531	21.6	39.5	75.3
β_2	3.090	1.129	2.022	0.562	0.251	1.039
β_4	2.367	1.833	0.807	0.315	−0.161	0.733
β_6	0.855	0.325	0.118	0.640	1.099	1.469
β_8	0.115	0.022	−0.036	−0.412	−0.523	−0.467
β_{10}	0.008	0.001	−0.006	−0.043	−0.059	−0.035
β_{12}				−0.005	−0.008	−0.016
β_{14}					−0.001	−0.003

[a]Cf. Eq. (29).

[b]Results in this column for He include the higher-order effects discussed in Sec. II D.

Our relative triply differential cross sections for the case $\theta_{12}=\pi$ and for equal energy sharing are shown for Ne, Ar, Kr, and Xe targets, respectively, in Figs. 4, 5, 6, and 7. Each figure gives our results for three excess energies: 4, 2, and 0.5 eV. Whenever possible, comparisons are made with the relative experimental measurements of Rösel *et al.* [7] and of Selles, Mazeau, and Huetz [8]. No other theoretical results are known to us.

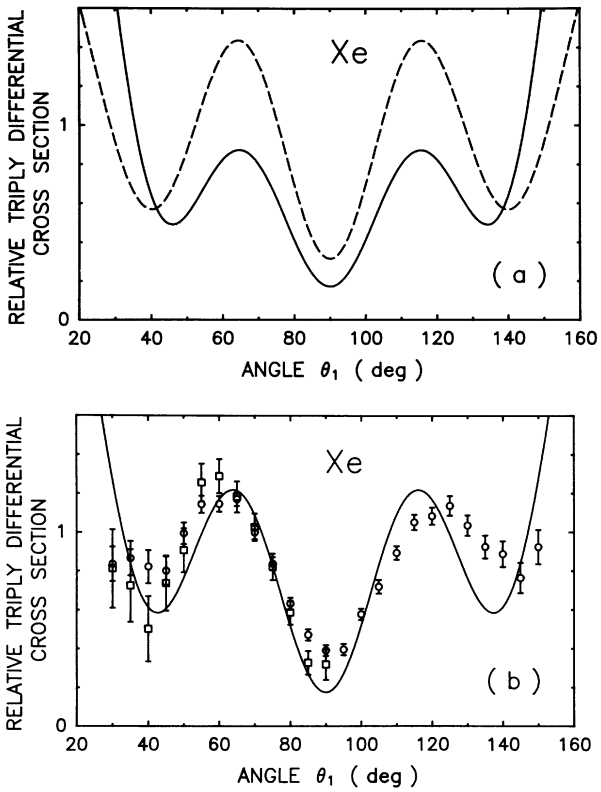

FIG. 7. Relative triply differential $(e,2e)$ cross sections for a Xe-atom target for final states having $\theta_{12}=\pi$ and the continuum electrons sharing the excess energy E_{ex} equally. (a) Solid curve: present theoretical results [cf. Eqs. (29) and (18)] for 4 eV excess energy; dashed curve: present theoretical results for 0.5 eV excess energy. (b) Solid curve: present theoretical results for 2 eV excess energy; open circles: experimental results of Rösel, Bar, Jung, and Ehrhardt, Ref. [7], for 2 eV excess energy above the $Xe^+(^2P_{3/2})$ thresholds; open squares: experimental results of Rösel *et al.*, Ref. [7], for 2 eV excess energy above the $Xe^+(^2P_{1/2})$ threshold.

1. *Comparison with results for H and He*

Before discussing each of the heavy rare-gas target results individually, it is interesting to compare them first with the results for H and for He targets. One sees immediately from Fig. 4 that the angular distribution for Ne is very similar to that for H. Furthermore, one sees from Figs. 5–7 that Ar, Kr, and Xe have two local maxima centered about $\theta_1=\pi/2$ in contrast to the single maximum observed in He at $\theta_1=\pi/2$.

It is useful to interpret these differences in terms of the dimensionless angular distribution asymmetry parameters β_λ defined in Eq. (29). For the case of 2 eV excess energy with equal energy sharing, our results for these parameters are presented in Table III for H, He, Ne, Ar, Kr, and Xe. We have chosen this value of E_{ex} since there is much experimental data available with which to compare our results. Furthermore the parameters β_λ in Table III will facilitate use of our results by other investigators. In particular, since we also give the value of σ in Table III, all parameters are given to construct our absolute triply differential cross sections [using Eq. (29)]. This should prove useful in the future when absolute experimental measurements become available.

One sees from Table III that H and Ne are similar in that β_2 is the largest asymmetry parameter. He is unique in that β_4 is its largest asymmetry parameter. Finally, Ar, Kr, and Xe are similar in that β_6 in their largest asymmetry parameter, although all of the asymmetry parameters β_2, β_4, β_6, and β_8 have significantly large magnitudes.

These differences in the relative magnitudes of the asymmetry parameters β_λ may in turn be traced to differences in importance of the various allowed scattering amplitudes $A_{RG}(lLS)$. From Eq. (18), we see from the two $3j$ symbols that $|L-L'|\leq\lambda\leq L+L'$ and $|l-l'|\leq\lambda\leq l+l'$. Furthermore, the pairs L,L' and l,l' must have the same parity. For Ne, the three largest am-

plitudes $A_{RG}(lLS)$ are those for $s(^3P)$, $p(^1D)$, and $d(^3F)$. Both of the latter two amplitudes contribute to β_2 as does the interference term involving the $s(^3P)$ and $d(^3F)$ amplitudes. For Ar, Kr, and Xe, the three largest amplitudes are those for $f(^1G)$, $p(^1D)$, and either $d(^3P)$ (for Ar) or $p(^1S)$ (for Kr and Xe). Furthermore, the $g(^3H)$ amplitude is significant also. Both the $f(^1G)$ and the $g(^3H)$ amplitudes contribute to the β_6 asymmetry parameter for these elements.

2. *Discussion of results for Ne, Ar, Kr, and Xe targets*

Our results in Fig. 4 for Ne show a decreasing minimum in the relative triply differential cross section as the excess energy decreases from 4 to 0.5 eV. This behavior stems primarily from a 59% decrease in the coefficient β_4 over this change in excess energy. For 4 eV excess energy, there is good quantitative agreement with the relative experimental measurements of Selles, Mazeau, and Huetz [8]. For 2 and 0.5 eV excess energy there is only qualitative agreement with experiment [8].

Our results in Fig. 5 for Ar show a very interesting change in the angular distribution as the excess energy decreases from 4 to 0.5 eV. Whereas there are two local maxima and a central minimum about $\theta_1=\pi/2$ for 4 and for 2 eV excess energy, there is only a rather flat-topped local maximum at $\theta_1=\pi/2$ for 0.5 eV excess energy. This behavior stems from a rapid increase in β_4 (from -0.18 to 1.2) combined with a simultaneous rapid decrease of β_6 (from 0.98 to 0.01) as the excess energy decreases from 4 to 0.5 eV. Agreement with the relative experimental results of Selles, Mazeau, and Huetz [8] is qualitatively good for $E_{ex}=4$ and 0.5 eV. For $E_{ex}=2$ eV, however, experiment [8] finds a local maximum at $\theta_1=\pi/2$ while theory predicts a local minimum. This disagreement for $E_{ex}=2$ eV may be interpreted as experimental evidence that the decrease of β_6 and the increase of β_4 occur more rapidly with decreasing E_{ex} than is predicted theoretically.

Our results in Fig. 6 for Kr show that the peak-to-trough amplitude for the two local maxima and the central minimum at $\theta_1=\pi/2$ decreases as the excess energy decreases from 4 to 0.5 eV. As in Ar, this decreasing amplitude stems from the simultaneous decrease of β_6 and increase of β_4 as the excess energy decreases. For $E_{ex}=4$ and 2 eV our results are in good qualitative agreement with both the experimental results of Selles, Mazeau, and Huetz [8] and those of Rösel, Bär, Jung, and Ehrhardt [7], although the theoretical peak-to-trough amplitude of oscillation is in each case larger than is found experimentally. For $E_{ex}=0.5$ eV, experiment finds a local maximum at $\theta_1=\pi/2$ while theory predicts a local minimum. This disagreement for $E_{ex}=0.5$ eV may be interpreted as experimental evidence that the decrease of β_6 and the increase of β_4 are more rapid with decreasing E_{ex} than predicted theoretically. Note that Selles, Mazeau, and Huetz [8] resolve the $Kr(^2P_{3/2})$ and $Kr(^2P_{1/2})$ thresholds but find that the angular distributions for the two thresholds are nearly the same. We show in Fig. 6 only their results for the $Kr(^2P_{3/2})$ threshold.

Our results in Fig. 7 for Xe show an increasing peak-to-trough amplitude for the two local maxima and the central minimum at $\theta_1=\pi/2$ as the excess energy decreases from 4 to 0.5 eV. This behavior stems from a relatively constant value of β_6 combined with rapidly decreasing values of β_2 and β_4 as E_{ex} decreases. In comparison with the relative experimental measurements of Rösel, Bär, Jung, and Ehrhardt [7], there is reasonably good quantitative agreement. Note how the experimental data of Rösel *et al.* [7] for the $Xe(^2P_{3/2})$ and $Xe(^2P_{1/2})$ thresholds are quite similar, as was the case for the data of Selles, Mazeau, and Huetz [8] for the fine-structure levels of Kr.

IV. SUMMARY AND CONCLUSIONS

In this paper we have provided a detailed description of our approach for describing the target dependence of the angular distributions for near-threshold $(e,2e)$ processes for final-state configurations in which $\theta_{12}=\pi$. For H and He we have provided a detailed analysis of the nonequal-energy-sharing case ($\varepsilon_1=3.5$ eV and $\varepsilon_2=0.5$ eV) that was first presented in Ref. [17]. We have also presented results for the equal-energy-sharing case for excess energies of 2 and 0.5 eV and compared our results with available experimental and other theoretical results. In particular, for He we have provided a detailed analysis of the effects of exchange and higher-order capture interactions on our results. We have also presented here results of more approximate distorted-wave theoretical calculations for the triply differential cross sections for $(e,2e)$ processes in Ne, Ar, Kr, and Xe for the case of $\theta_{12}=\pi$ and equal energy sharing of 4, 2, and 0.5 eV excess energy. These triply differential theoretical $(e,2e)$ results for these heavier rare-gas targets were shown to be generally in reasonable qualitative agreement with available experimental results. Finally, for the case of 2 eV excess energy with equal energy sharing, we have presented in Table III the parameters σ and β_λ from which other researchers may construct our absolute triply differential cross sections for all of the targets considered: H, He, Ne, Ar, Kr, and Xe.

Among our key conclusions is the fact that short-range effects on the s-wave phase shifts of both incident and final-state continuum electrons are the reason for the qualitatively different behaviors of the $(e,2e)$ angular distributions for H and for He targets. In particular, exchange and higher-order capture processes are shown to affect the triply differential cross sections for He quantitatively but not qualitatively. We also note (as have Jones, Madison, and Srivastava [18]) that the three theoretical calculations [16–18] for near-threshold $(e,2e)$ processes in H, while differing only in detail for the relative triply differential cross section for H, differ significantly for the absolute triply differential cross section for H. Significant differences in the absolute cross sections for He also have been shown. Absolute $(e,2e)$ experimental measurements are needed to help sort out these differences. Finally, for the $(e,2e)$ angular distributions for the heavier rare-gas targets Ne, Ar, Kr, and Xe our results appear in general to be in qualitative agree-

ment with available relative experimental measurements. In the few instances where there are qualitative differences between our results and experiment, it appears these stem from the fact that changes in the angular distribution as a function of the excess energy E_{ex} are predicted theoretically to occur more slowly with decreasing E_{ex} than observed experimentally.

In conclusion, we mention finally that our emphasis here has been on target effects on $(e,2e)$ angular distributions near threshold and not on the energy dependence of the absolute triply differential cross section near threshold. Indeed, by replacing the true Coulomb interaction between the two outgoing electrons by variationally determined screening potentials [26–28] we exclude the possibility of obtaining the correct energy dependence of the triply differential cross sections near threshold, which is the subject of the Wannier-Peterkop-Rau (WPR) theory [9–12]. As discussed by Selles, Mazeau, and Huetz [8], the WPR theory applied to the triply differential $(e,2e)$ cross section for the $\theta_{12}=\pi$ geometry has a cross section near threshold proportional to $E_{ex}^{-0.373}$. However, the range of validity of the WPR theory is uncertain and thus it is not clear whether it applies in the energy range $0.5 \leq E_{ex} \leq 4$ eV that we have considered here. For all of these reasons we have not focused on the energy dependence of our absolute triply differential cross sections.

ACKNOWLEDGMENTS

We gratefully acknowledge discussions and correspondence with P. L. Altick, M. Brauner, J. S Briggs, H. Ehrhardt, U. Fano, L. Frost, A. Huetz, S. Jones, D. H. Madison, J. Mazeau, and T. Rösel. This work was supported in part by NSF Grant No. PHY-9108002.

APPENDIX

1. Wave functions for the continuum states

The approximate single-particle Hamiltonian for the radial wave functions used in this work is

$$h_l=-\frac{1}{2}\frac{d^2}{dr^2}-\frac{Z}{r}+\frac{l(l+l)}{2r^2}+V_{HF} , \tag{A1}$$

where V_{HF} is a Hartree-Fock (HF) potential describing electronic interactions. In this work the ground-state target wave functions are evaluated using the computer program MCHF77 [36]. The same one-electron wave functions are used to construct the wave function of the final-state ionic core. Each radial continuum wave function $P_{\varepsilon l}$ in the initial- and final-state wave functions in Eqs. (10) and (11) is evaluated using a potential $V_{\varepsilon l}$ which is dependent on the angular momentum coupling of the total wave functions in these equations. This potential is derived from the variational principle,

$$\delta\langle\Psi_f(\cdots L_T M_T \cdots S_T M_{S_T})|H|\Psi_i(\cdots L_T M_T \cdots S_T M_{S_T})\rangle=0 , \tag{A2}$$

by keeping those terms involving interactions between the εl state and the occupied bound states.

For each value of the continuum electron's orbital angular momentum l, if there exist occupied electron orbitals with the same l in the target atom, the orthogonality between the wave functions of these bound electrons and the partial waves of the incident and outgoing continuum electrons is ensured by constructing a single Hermitian potential [37–41]

$$V_{HF}=V_{g,l}+(1-P_l)(V_{\varepsilon l}-V_{g,l})(1-P_l) , \tag{A3a}$$

where $P_l=\sum_i|n_i l\rangle\langle n_i l|$, with the summation running over the occupied states of the target, and where $V_{g,l}$ is the potential used for these occupied states. Otherwise

$$V_{HF}=V_{\varepsilon l} \tag{A3b}$$

is used in Eq. (A1).

Since the HF potentials $V_{g,l}$ for the ground-state orbitals of atoms as well as the potential terms describing the interaction of a continuum electron with closed subshells are given in standard references [42,43], the expressions for $V_{g,l}$ are not given here, and in the expressions for $V_{\varepsilon l}$ given below, terms related to closed subshells are not given except when needed for comparisons. Such terms are of course included in our calculation. The potentials $V_{\varepsilon l}$ used in this work are listed as linear combinations of operators J_{nl}^{λ} and K_{nl}^{λ} defined through [41]

$$J_{nl}^{\lambda}P_{n'l'}(r)=y_{\lambda}(nl,nl;r)P_{n'l'}(r) , \tag{A4}$$

$$K_{nl}^{\lambda}P_{n'l'}(r)=y_{\lambda}(nl,n'l';r)P_{nl}(r) , \tag{A5}$$

where the two-electron integral y_{λ} has been defined in Eq. (6).

The potentials used for the partial-wave functions $P_{\varepsilon l}(r)$ of the incident electron are given in Eqs. (A6) and (A7) below. Since for rare-gas targets these potentials contain only interactions with closed subshells, only the potential for He is presented here as an example:

$$V_{\varepsilon l}^{H}=J_{1s}^{0}+(-1)^{S}[l]^{-1}K_{1s}^{l} , \tag{A6}$$

$$V_{\varepsilon l}^{He}=2J_{1s}^{0}-[l]^{-1}K_{1s}^{l} . \tag{A7}$$

The potentials used for the wave functions $P_{\varepsilon_i l}$ $(i=1,2)$ for the final-state continuum electrons are given in Eqs. (A8), (A9), and (A10) below for the cases of H, He, and other rare gases, respectively,

$$V_{\varepsilon_i l}^{H}=\Delta_i J_{1s}^{0} . \tag{A8}$$

$$V_{\varepsilon_i l}^{He}=(1+\Delta_i)J_{1s}^{0}-(-1)^{S}2^{-1}[l]^{-1}K_{1s}^{l} . \tag{A9}$$

$$V_{\varepsilon_i l}^{RG}=(5+\Delta_i)J_{n_0 p}^{0}-3l[l-1]^{-1}[l]^{-1}K_{n_0 p}^{l-1} -3(l+1)[l]^{-1}[l+1]^{-1}K_{n_0 p}^{l+1} . \tag{A10}$$

In Eq. (A10), $n_0=2,3,4,5$ for Ne, Ar, Kr, and Xe, respectively, and interactions with closed subshells are not listed but are understood to be included. In Eqs. (A8)–(A10), Δ_i $(i=1,2)$ represents the effective screening charge defined in Eq. (4), where the function $y_0(r)$, which is defined in Eq. (5) and in the text following it, is designated here by $J^0_{n_0l_0}$ [cf. Eqs. (6) and (A4)].

Neglecting the screening charge Δ_i, Eqs. (A9) and (A10) define potentials for the $\varepsilon_i l$ state that are approximations to a more general formula for electron-impact ionization of a closed subshell $n_0 l_0^{4l_0+2}$ derived from Eq. (A2) with respect to $\delta P_{\varepsilon_1 l_1}(r)$, namely,

$$
\begin{aligned}
V(LS,L'S')=&\delta_{LL'}\delta_{SS'}(2[l_0]-1)J^0_{n_0l_0}\\
&-\delta_{SS'}\sum_{\lambda>0}J^{\lambda}_{n_0l_0}(-1)^{L+L'+L_T+l_2}[l_0][l_1]([L][L'])^{1/2}\begin{Bmatrix}l_0&\lambda&l_0\\0&0&0\end{Bmatrix}\begin{Bmatrix}l_1&\lambda&l_1\\0&0&0\end{Bmatrix}\begin{Bmatrix}l_0&L&L_T\\L'&l_0&\lambda\end{Bmatrix}\begin{Bmatrix}l_1&L&l_2\\L'&l_1&\lambda\end{Bmatrix}\\
&-\sum_{\lambda}K^{\lambda}_{n_0l_0}(-1)^{\lambda+l_0+l_1}[l_0]\begin{Bmatrix}l_0&\lambda&l_1\\0&0&0\end{Bmatrix}^2\\
&\times\left[\delta_{LL'}\delta_{SS'}-(-1)^{S+S'}2^{-1}[l_1]([L][L'][S][S'])^{1/2}\begin{Bmatrix}l_1&l_2&L\\L_T&l_0&\lambda\end{Bmatrix}\begin{Bmatrix}l_1&l_2&L'\\L_T&l_0&\lambda\end{Bmatrix}\right]. \qquad \text{(A11)}
\end{aligned}
$$

For He, Eq. (A11) simplifies substantially since $l_0=0$; in order to obtain Eq. (A9) we simply neglected off-diagonal terms which couple singlet and triplet states. For the other rare gases, which have $l_0=1$, we obtained Eq. (A10) by only keeping those terms in Eq. (A11) which have the factor $\delta_{LL'}\delta_{SS'}$.

2. Amplitudes $A_{\rm H}$, $A_{\rm He}$, and $A_{\rm RG}$

These amplitudes, which are used in Eqs. (17)–(19), are defined in Eq. (15). Expressions for the matrix element in Eq. (15) will be given as $\langle V\rangle_{\rm H}$, $\langle V\rangle_{\rm He}$, and $\langle V\rangle_{\rm RG}$ for the cases of H, He, and the other rare gases, respectively. These matrix elements are expressed in terms of Slater integrals

$$R^{\lambda}(a,b;c,d)=\int_0^{\infty}P_b(r)P_d(r)y_{\lambda}(a,c;r)dr\ , \qquad \text{(A12)}$$

where $y_{\lambda}(a,c;r)$ is defined in Eq. (6).

For the case of H,

$$
\begin{aligned}
\langle V\rangle_{\rm H}=&(-1)^{l}([l_1][l_2])^{1/2}\begin{Bmatrix}l_1&l_2&l\\0&0&0\end{Bmatrix}\\
&\times\{[l_1]^{-1}R^{l_1}(\varepsilon_1l_1,\varepsilon_2l_2;1s,\varepsilon l)\\
&+(-1)^{S}[l_2]^{-1}R^{l_2}(\varepsilon_2l_2,\varepsilon_1l_1;1s,\varepsilon l)\}\ . \qquad \text{(A13)}
\end{aligned}
$$

For the case of He, using $\langle V\rangle_{\rm H}$ in Eq. (A13) to denote terms which are identical in form with those for the case of H, we have

$$\langle V\rangle_{\rm He}=(-1)^{S+1}(2^{-1}[S])^{1/2}\langle V\rangle_{\rm H}\ . \qquad \text{(A14)}$$

When Eqs. (A13) and (A14) as well as the appropriate S_0 and S_T values for the two cases are substituted into Eq. (15), the expression for $A_{\rm He}$ differs in form from that for $A_{\rm H}$ by only an extra factor of $(-1)^{S+1}\sqrt{2}$.

For the other rare gases, the matrix elements are a special case (e.g., the case $l_0=1$) of those describing electron-impact ionization of a closed subshell $n_0 l_0^{4l_0+2}$,

$$
\begin{aligned}
\langle V\rangle_{\rm RG}=&(2^{-1}[S][l_0][l_1][l_2][L])^{1/2}\\
&\times\sum_{\lambda}(-1)^{\lambda+1}\left[(-1)^{l_1+l_2+S}\begin{Bmatrix}l_1&\lambda&l_0\\0&0&0\end{Bmatrix}\begin{Bmatrix}l_2&\lambda&l\\0&0&0\end{Bmatrix}\begin{Bmatrix}l_1&l_2&L\\l&l_0&\lambda\end{Bmatrix}\right.\\
&\times R^{\lambda}(\varepsilon_1l_1,\varepsilon_2l_2;n_0l_0,\varepsilon l)+(-1)^{L}\begin{Bmatrix}l_1&\lambda&l\\0&0&0\end{Bmatrix}\begin{Bmatrix}l_2&\lambda&l_0\\0&0&0\end{Bmatrix}\\
&\left.\times\begin{Bmatrix}l_1&l_2&L\\l_0&l&\lambda\end{Bmatrix}R^{\lambda}(\varepsilon_2l_2,\varepsilon_1l_1;n_0l_0,\varepsilon l)\right]. \qquad \text{(A15)}
\end{aligned}
$$

3. Second-order corrections to T_{fi}

When the second-order term in Eq. (28) is included in the calculation for the case of He targets, the expression for $\langle V\rangle_{\rm He}$ [cf. Eqs. (A13) and (A14)] acquires an additional term $v^{(2)}$ in the curly brackets in Eq. (A13),

$$v^{(2)}=[l_1]^{-2}R^{l_1}(1s,\varepsilon_2 l_2;\Lambda l_1,\varepsilon l)+(-1)^S[l_2]^{-2}R^{l_2}(1s,\varepsilon_1 l_1;\Lambda l_2,\varepsilon l)$$
$$-\delta_{S0}2[l]^{-1}\{[l_1]^{-1}R^{l}(1s,\varepsilon_2 l_2;\varepsilon l,\Lambda l_1)+[l_2]^{-1}R^{l}(1s,\varepsilon_1 l_1;\varepsilon l,\Lambda l_2)\}$$
$$+\delta_{S0}\delta_{l0}\delta_{l_1 l_2}2[l_1]^{-1}(2\varepsilon_{1s}-\varepsilon_1-\varepsilon_2)^{-1}R^{0}(1s,1s;1s,\varepsilon s)R^{l_1}(\varepsilon_1 l_1,\varepsilon_2 l_1;1s,1s)\ . \tag{A16}$$

In Eq. (A16), the functions $P_{\Lambda l_i}(r)$ $(i=1,2)$ are solutions of the inhomogeneous differential equation [44,45]

$$(2\varepsilon_{1s}-\varepsilon_i-h_{l_i})P_{\Lambda l_i}(r)=(1-\delta_{l_i 0}|1s\rangle\langle 1s|)y_{l_i}(\varepsilon_i l_i,1s;r)P_{1s}(r)\ , \tag{A17}$$

where h_{l_i} is defined in Eq. (A1) and $y_{l_i}(\varepsilon_i l_i,1s;r)$ is defined in Eq. (6). All of the terms in Eq. (A16) are due to initial-state correlations; those terms having δ_{S0} may be identified as capture interactions.

[1] *Electron Impact Ionization,* edited by T. D. Märk and G. H. Dunn (Springer, New York, 1985).
[2] H. Ehrhardt, K. Jung, G. Knoth, and P. Schlemmer, Z. Phys. D **1**, 3 (1986).
[3] F. W. Byron, Jr. and C. J. Joachain, Phys. Rep. **179**, 211 (1989).
[4] A. Lahmam-Bennani, J. Phys. B **24**, 2401 (1991).
[5] P. Selles, A. Huetz, and J. Mazeau, J. Phys. B **20**, 5195 (1987).
[6] P. Schlemmer, T. Rösel, K. Jung, and H. Ehrhardt, Phys. Rev. Lett. **63**, 252 (1989).
[7] T. Rösel, R. Bär, K. Jung, and H. Ehrhardt, in *Invited Papers and Progress Reports, European Conference on (e,2e) Collisions and Related Problems,* edited by H. Ehrhardt (Universität Kaiserslautern, Kaiserslautern, Germany, 1989), pp. 69–81.
[8] P. Selles, J. Mazeau, and A. Huetz, J. Phys. B **23**, 2613 (1990).
[9] G. H. Wannier, Phys. Rev. **90**, 817 (1953).
[10] A. R. P. Rau, Phys. Rev. A **4**, 207 (1971); Phys. Rep. **110**, 369 (1984).
[11] R. Peterkop, J. Phys. B **4**, 513 (1971); **16**, L587 (1983).
[12] See also J. M. Feagin, J. Phys. B **17**, 2433 (1984), and references therein.
[13] H. Klar and W. Schlecht, J. Phys. B **9**, 1699 (1976).
[14] C. H. Greene and A. R. P. Rau, Phys. Rev. Lett. **48**, 533 (1982); J. Phys. B. **16**, 99 (1983).
[15] A. D. Stauffer, Phys. Lett. **91A**, 114 (1982).
[16] M. Brauner, J. S. Briggs, H. Klar, J. T. Broad, T. Rösel, K. Jung, and H. Ehrhardt, J. Phys. B **24**, 657 (1991).
[17] C. Pan and A. F. Starace, Phys. Rev. Lett. **67**, 185 (1991).
[18] S. Jones, D. H. Madison, and M. K. Srivastava, J Phys. B (to be published).
[19] M. Brauner, J. S. Briggs, and H. Klar, J. Phys. B **22**, 2265 (1989).
[20] Reference [7], Fig. 1. This figure is published as Fig. 4 of Ref. [4].
[21] K. N. Huang, Phys. Rev. A **28**, 1869 (1983).
[22] P. L. Altick, J. Phys. B **18**, 1841 (1985).
[23] A. Messiah, *Quantum Mechanics* (Wiley, New York, 1966), Vol. II, pp. 822–825; P. Roman, *Advanced Quantum Theory* (Addison-Wesley, Reading, MA, 1965), pp. 370–377.
[24] C. Froese-Fischer, *The Hartree-Fock Method for Atoms* (Wiley, New York, 1977).
[25] P. J. Redmond (unpublished). Redmond's results have been presented without derivation by L. Rosenberg, Phys. Rev. D **8**, 1833 (1973). A recent derivation is presented in Ref. [19].
[26] M. R. H. Rudge and M. J. Seaton, Proc. R. Soc. London, Ser. A **283**, 262 (1965).
[27] R. K. Peterkop, *Theory of Ionization of Atoms by Electron Impact* (Colorado Associated University Press, Boulder, 1977), pp. 128 and 129.
[28] S. Jetzke, J. Zaremba, and F. H. M. Faisal, Z. Phys. D **11**, 63 (1989); F. H. M. Faisal, in *Atoms in Strong Fields,* edited by C. A. Nicolaides, C. W. Clark, and M. H. Nayfeh (Plenum, New York, 1990), pp. 407–424.
[29] Cf., e.g., A. F. Starace, in *Handbuch der Physik 31,* edited by W. Mehlhorn (Springer, Berlin, 1982), Eq. (4.27).
[30] Cf., e.g., A. F. Starace, in Ref. [29], pp. 8–15.
[31] A. R. Edmonds, *Angular Momentum in Quantum Mechanics,* 2nd ed. (Princeton University Press, Princeton, NJ, 1960), Eq. 4.6.5.
[32] A. P. Yutisis, I. B. Levinson, and V. V. Vanagas, *Theory of Angular Momentum* (Israel Program for Scientifc Translations, Washington, DC, 1962), Eq. (A.7.4).
[33] Cf. A. R. Edmonds, Ref. [31], Eq. 4.6.6.
[34] This property is known as Brillouin's Theorem. See, e.g., I. Lindgren and J. Morrison, *Atomic Many-Body Theory* (Springer, Berlin, 1982), Sec. 5.4.
[35] Cf. Fig. 1 of Ref. [7]; presented also in Fig. 6(b) of Ref. [16].
[36] C. Froese-Fischer, Comput. Phys. Commun. **14**, 145 (1978).
[37] L. M. Frantz, R. L. Mills, R. G. Newton, and A. M Sessler, Phys. Rev. Lett. **1**, 340 (1958).
[38] B. A. Lippmann, M. H. Mittleman, and K. M. Watson, Phys. Rev. **116**, 920 (1959).
[39] R. T. Pu and E. S. Chang, Phys. Rev. **151**, 31 (1966).
[40] H. J. Silverstone and M. L. Yin, J. Chem. Phys. **49**, 2026 (1968).
[41] S. Huzinaga and C. Arnau, Phys. Rev. A **1**, 1285 (1970).
[42] I. Lindgren and J. Morrison, Ref. [34], Eqs. (3.50), (6.41), (6.43), and (7.20).
[43] E. U. Condon and G. H. Shortley, *The Theory of Atomic Spectra* (Cambridge University Press, New York, 1951), Chap. VI.
[44] R. M Sternheimer, Phys Rev. **84**, 244 (1951).
[45] A. Dalgarno and J. T. Lewis, Proc. R. Soc. London, Ser. A **233**, 70 (1955).